Cerebral Cortex June 2010;20:1448-1461
doi:10.1093/cercor/bhp208
Advance Access publication October 12, 2009

Cytoarchitecture and Probabilistic Maps of the Human Posterior Insular Cortex

Florian Kurth[1,2], Simon B. Eickhoff[1–4], Axel Schleicher[1], Lars Hoemke[2], Karl Zilles[1–3] and Katrin Amunts[2–4]

[1]C. & O. Vogt Institute of Brain Research, University Düsseldorf, 40225 Düsseldorf, Germany, [2]Institute for Neuroscience and Medicine (INM-1, INM-2), Research Centre Jülich, 52425 Jülich, Germany, [3]JARA—Translational Brain Medicine, 52425 Jülich, Germany and [4]Department of Psychiatry and Psychotherapy, RWTH Aachen University, 52074 Aachen, Germany

The human posterior insula was shown to respond to a wide variety of stimulation paradigms (e.g. pain, somatosensory, or auditory processing) in functional imaging experiments. Although various anatomical maps of this region have been published over the last century, these schemes show variable results. Moreover, none can directly be integrated with functional imaging data. Hence, our current knowledge about the structure–function relationships in this region remains limited. We therefore remapped the posterior part of the human insular cortex in 10 postmortem brains using an observer-independent approach. This analysis revealed the existence of 3 cytoarchitectonically distinct areas in the posterior insula. The examined brains were then 3D reconstructed and spatially normalized to the Montreal Neurological Institute single-subject template. Probabilistic maps for each area were calculated by superimposing the individual delineations, and a cytoarchitectonic summary map was computed to chart the regional architectonic organization. These maps can be used to identify the anatomical correlates of functional activations observed in neuroimaging studies and to understand the microstructural correlates of the functional segregation of the human posterior insula.

Keywords: areas, dysgranular, granular, microstructure, sensory

Introduction

The human insular cortex is located in the depth of the Sylvian fissure and covered by the frontal, parietal, and temporal opercular lobes due to the differential growth patterns of these regions during ontogenesis. It is demarcated from the adjacent parts of the cortex by the circular sulcus of Reil consisting of the superior limiting part (macroscopic border toward the frontoparietal operculum) and an inferior limiting sulcus (macroscopic border toward the temporal lobe) (Mesulam and Mufson 1985; Zilles 2004). Commonly, 5–7 sulci running in a radial orientation toward the insular pole are distinguished (Morgane et al. 1980; Ono et al. 1990; Naidich et al. 2004), which divide the insula into 2 long, 2–3 short, and a variable accessory gyrus. The central sulcus of the insula is considered to represent the border between the anterior and the smaller posterior insula. The latter region, which is the focus of the present analysis, consists of the anterior and posterior long gyrus separated by the insular postcentral sulcus (von Economo and Koskinas 1925; Naidich et al. 2004).

In neuroimaging experiments using functional magnetic resonance imaging (fMRI) or positron emission tomography, the posterior insula has been implicated in the cortical processing of a wide variety of different stimuli. In particular, this region was repeatedly shown to process painful (Ostrowsky et al. 2002; Frot and Mauguiere 2003; Alkire et al. 2004; Baumgärtner et al. 2006), thermosensory (Craig et al. 2000; Hua et al. 2005), auditory (Bamiou et al. 2003), vestibular stimuli (Fasold et al. 2002; Fink et al. 2003), and motor tasks (Johansen-Berg and Matthews 2002; Carey et al. 2005; Loubinoux et al. 2007).

The microstructure of the human insula, that is, the putative anatomical substrate of these functions, has repeatedly been studied over the last century. Some classical publications (Brodmann 1909; von Economo and Koskinas 1925) distinguished a posterior granular and an anterior dysgranular or agranular part separated by the central insular sulcus (Fig. 1), whereas others (Vogt C and Vogt O 1919; Rose 1928) reported a more detailed parceling of this region based on a comparison with nonhuman primates and by combining cytoarchitecture and myeloarchitecture. In a recent, very influential scheme based on work in nonhuman primates (Mesulam and Mufson 1985), the concept of "granularity" (presence and characteristics of an inner granular layer) was proposed as a key feature for the architectonic subdivision of the insular lobe (Fig. 2). The resulting map describes a circular organization of cortical areas around the insular pole. In particular, a central allocortical polar region is encircled by an agranular belt, which is again enclosed by a dysgranular one. The posterior insula is covered by a granular region bordered by the dysgranular belt.

The question how the reported functional diversity of the posterior insula maps to its architectonic structure is yet unresolved as a direct comparison of classical brain maps and functional imaging data are problematical for several reasons: First of all, it has to be emphasized that all classical architectonic maps purely relied on visual inspection of histological sections, using subjective nonstandardized criteria and very small sample sizes. This presumably led to the differences in the available maps described above, which evidently question the generalizability of such maps for anatomical reference (Zilles et al. 2003). Second, classical cytoarchitectonic maps are only available as schematic drawings and hence cannot be matched with the 3D data sets resulting from neuroimaging experiments. Furthermore, these atlases also lack information about intersubject variability in the size and extent of cortical areas provoking the misleading view that a particular cortical location is necessary and in all subjects corresponding to a particular area. Finally, it has to be emphasized that most influential anatomical data in the insular cortex are derived from studies in nonhuman primates (Mesulam and Mufson 1985). Though a basic comparability between the insular cortex of humans and nonhuman primates can be assumed, straightforward extrapolations must be discussed with caution.

The aim of the present study was therefore to analyze the cytoarchitecture of the human posterior insula in serial

© The Author 2009. Published by Oxford University Press. All rights reserved.
For permissions, please e-mail: journals.permissions@oxfordjournals.org

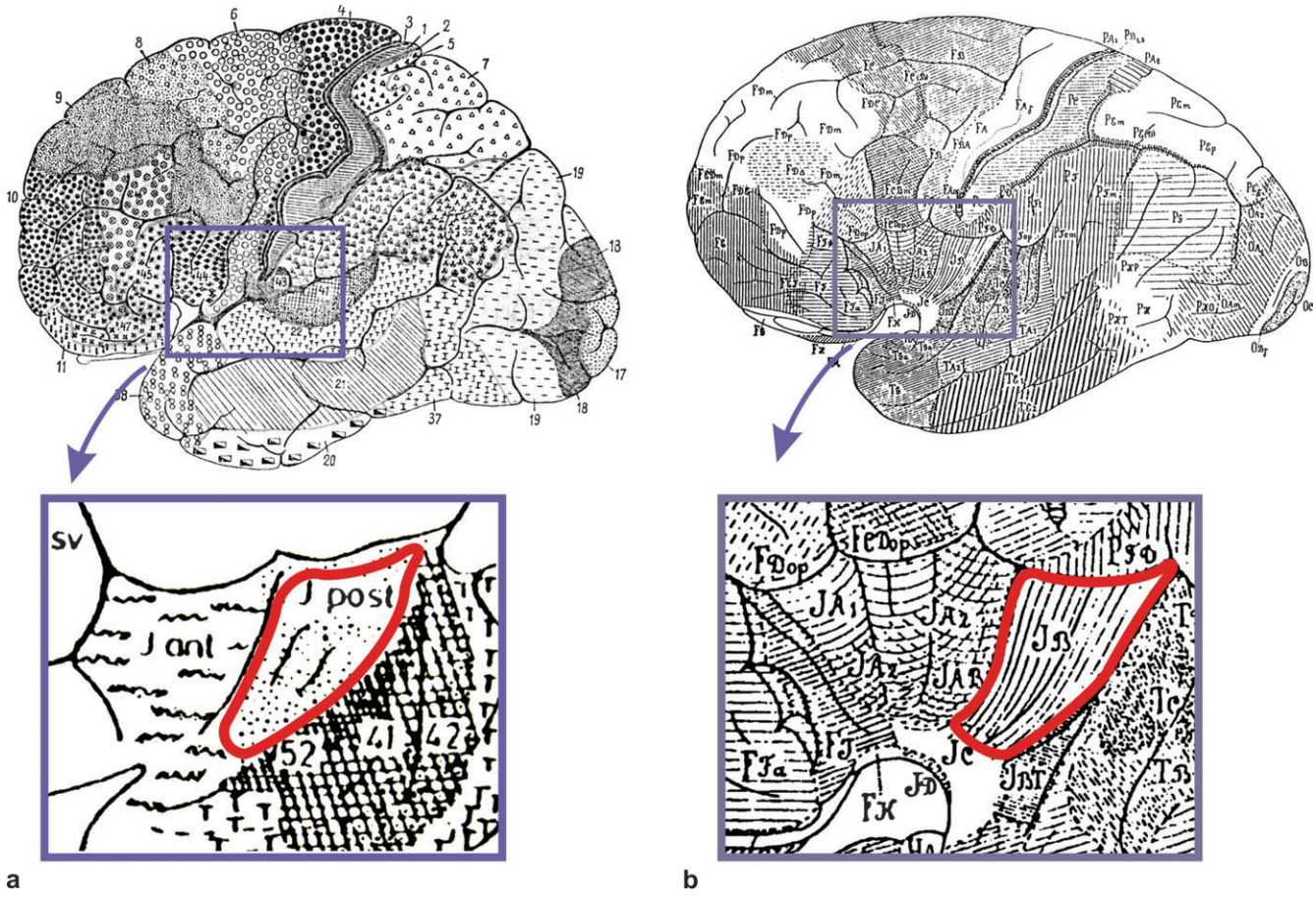

Figure 1. Classical cytoarchitectonic maps by (*a*) Brodmann (1909) and (*b*) von Economo and Koskinas (1925). The posterior granular area is marked in red.

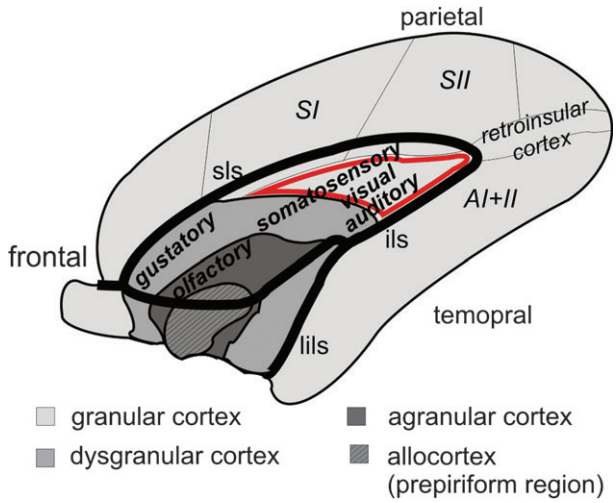

Figure 2. Schematic map of the macaque insula modified after Mesulam and Mufson (1985). AI + AII, primary and secondary auditory cortex; ils, inferior limiting sulcus; lils, lateral branch of the inferior limiting sulcus; sls, superior limiting sulcus; SI + SII, primary and secondary somatosensory cortex.

histological sections of 10 human postmortem brains using a statistical approach for the observer-independent detection of borders between cortical areas (Schleicher et al. 2005). The results of this mapping study will then be described by quantitative probability maps in standard stereotaxic space (Zilles et al. 2002; Toga et al. 2006) compatible with functional imaging data.

Material and Methods

Ten human postmortem brains (5 males and 5 females; see Table 1) of subjects without a clinical history of neurological or psychiatric diseases were obtained from the body donor program of the Anatomical Institute of the University of Düsseldorf according to legal requirements. Handedness was unknown, but assuming a 90% incidence of right-handedness (Annett 1973), most subjects should have been right-handed. The brains were removed from the skull within 24 h after death and fixed in formalin or Bodian's fixative for about 6 months. They were then scanned with a T_1-weighted 3D FLASH sequence (flip angle 40°, repetition time = 40 ms, time echo = 5 ms) using a Siemens 1.5-T scanner (Erlangen, Germany) to obtain 3D data sets documenting brain size and shape. Subsequently, the whole brains were embedded in paraffin and serially cut into coronary sections of 20 μm thickness. Every 15th section was stained for cell bodies using a silver staining method (Merker 1983) optimized to yield a high contrast between darkly stained cell bodies and light neuropil. Every fourth stained section (60th overall) was then analyzed, resulting in a distance of 1.2 mm between examined sections (Fig. 3).

Observer-Independent Detection of Cortical Borders

Cortical borders were identified using the approach described in detail by Schleicher et al. (2005). In short, rectangular regions of interest covering the posterior insula and neighboring cortex were defined in the histological sections, digitized in a meander-like sequence

using a motorized scanning microscope (KS-400; Zeiss, Oberkochen, Germany) and a CCD camera (Sony, Tokyo, Japan, resolution $1.01 \times 1.01\ \mu m^2$ per pixel), and transformed into gray-level index (GLI) images. In these images, the values of individual pixels summarize the areal fraction of darkly stained cell bodies in the corresponding measuring field as estimated by adaptive thresholding (Schleicher and Zilles 1990). Equidistant GLI profiles were then extracted perpendicular to the cortical layers (see Schleicher et al. 2000) between the layer I/II border (outer boundary) and the transition between layer VI and the white matter (inner boundary). These profiles hence quantify the regional shape of the laminar cell density pattern (Eickhoff, Schleicher, et al. 2007). The shape of each profile was quantified by a vector of 10 features based on central moments (mean GLI, mean X, standard deviation [SD], skewness, and kurtosis of the profile and their derivatives; Dixon et al. 1988; Zilles et al. 2002).

Differences between feature vectors indicate differences in the profile shape, that is, in cytoarchitecture, and were measured using the Mahalanobis distance (Mahalanobis et al. 1949; Schleicher et al. 2005). To increase the signal to noise ratio, distances were calculated between average feature vectors obtained from blocks of b ($8 \leqslant b \leqslant 20$) adjacent profiles instead of individual profiles. They were analyzed in a sliding window technique as a function of the profile number of the border between the blocks (Fig. 4). Maxima of this distance function revealed those positions where the regions covered by the 2 blocks showed the most dissimilar laminar patterns. The significance of these maxima was evaluated by a Hotelling's T^2-test with Bonferroni correction for multiple comparisons (Fig. 4). The position of a significant maximum was interpreted as a cortical border, if 1) it was consistently present across multiple block sizes, that is, widths of the sliding window, 2) no higher maximum was found within one block size at either side, and 3) that maximum could be reproduced at comparable positions in adjacent sections. These criteria in combination with the statistical assessment of the Mahalanobis distance function allowed discharging local inhomogeneities in cytoarchitecture revealing only borders between distinct cortical areas.

Table 1
Brains used for the analysis of the posterior insula

Case no.	Brain no.	Age in years	Gender	Cause of death	Fixative
4	207/84	75	M	Toxic glomerulonephritis	Formalin
5	382/81	59	F	Cardiorespiratory insufficiency	Formalin
6	16/96	54	M	Myocardial infarction	Formalin
7	146/86	37	M	Right heart failure	Formalin
9	68/95	79	F	Cardiorespiratory insufficiency	Bodian
10	2/95	85	F	Mesenteric artery infarction	Bodian
11	139/95	74	M	Myocardial infarction	Formalin
12	14/94	43	F	Pulmonary embolism	Formalin
13	2431	39	M	Drowning	Formalin
14	71/86	86	F	Cardiorespiratory insufficiency	Formalin

Note: M, male; F, female.

Interareal, Interhemispheric, and Interindividual Differences

For further characterization of the resulting cytoarchitectonic areas, we analyzed differences in cytoarchitecture and volumes between all areas. For each subject, area, and hemisphere, approximately 80 individual profiles were sampled evenly throughout its extent for further statistical analysis. All extracted profiles were obtained from regions that were free of histological artifacts and showed a perpendicular orientation of the sectioning plane to the cortical surface. From this sample of profiles, mean feature vectors were calculated for each subject, area, and hemisphere to quantify the individual areal-specific cytoarchitecture. Such mean cytoarchitectonic profiles were obtained for all delineated areas in the posterior insula and, in addition, also for the anteriorly adjacent agranular insular cortex. The similarity in cytoarchitectonic pattern between these areas—as indicated by their mean profiles—was assessed by a hierarchical cluster analysis based on profile shape. To this end, the feature vectors extracted from the GLI profiles were transformed to z-scores in order to make the features with their different metrics comparable. Subsequently, they were averaged across hemispheres for each area and side resulting in 8 areal feature vectors. The hierarchical cluster analysis was based on these feature vectors and used the Euclidean distance measure and the Ward linkage procedure (Dombrowski et al. 2001; Amunts et al. 2007). To statistically establish different clusters, the root mean square standard deviation (RMSSTD) index was applied (Sharma 1995), and the Euclidean distances for intracluster and intercluster differences were calculated. Interindividual and interareal differences in laminar pattern were assessed using a multivariate repeated measurement analysis of variance (ANOVA) with area and side (hemisphere) as within factors and subject as blocking factor in order to eliminate the marked interindividual variability. The analysis comprised 80 individual mean feature vectors (comprising brains, 2 hemispheres, and 4 areas). Due to the small sample size (resulting in too few degrees of freedom), the putative confounding variables age, gender, and side were analyzed in a separate ANOVA and a multivariate regression analysis.

The histological volumes (in cubic millimeters) of the delineated areas in the left and right hemispheres were calculated from area measurements (A_i) in images of the individual histological section (i) using the formula $V = s \times x \times y \times \sum A_i \times F$, where s is the distance between 2 measured sections (1.2 mm), x and y are the width and height of a pixel in the image (0.02116 mm each), and $\sum A_i$ is the sum of areas across all i evaluated sections (in pixels). F is the individual shrinkage factor of each brain calculated as ratios between the fresh volume of a brain and the volume reconstructed from its histological sections. The fresh volumes are the fresh weight of the brain × its mean specific density of 1.033 (Kretschmann et al. 1982). The resulting volumetric data were investigated by a repeated measurement ANOVA using the following design—between-subject factor: gender; within-subject factors: area and side; and blocking factor: subject.

Computation of Probabilistic Cytoarchitectonic Maps

The histological volumes of the brains were 3D reconstructed (Amunts et al. 2004) using 1) the 3D magnetic resonance imaging scan, 2) the

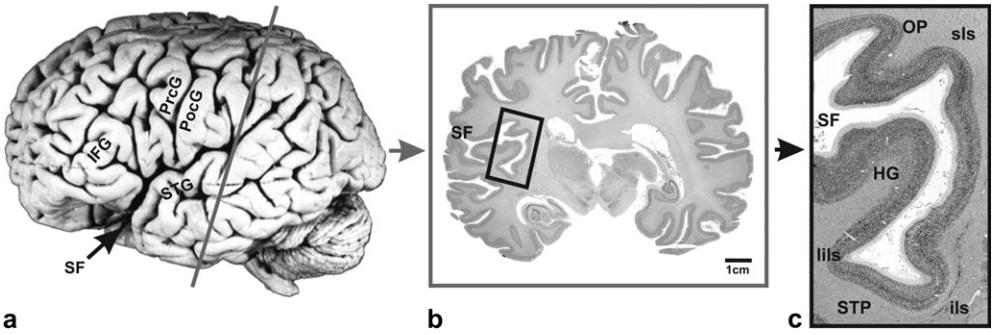

Figure 3. (*a*) Postmortem brain sectioned in the coronal plane. (*b*) Cell body–stained coronal section (20 μm) through the brain shown in (*a*). The position of the section is indicated by the line in (*a*). The region of interest (ROI) is marked in black. (*c*) ROI with anatomic landmarks as indicated by the box in (*b*). HG, Heschl's gyrus; IFG, inferior frontal gyrus; OP, operculum; PocG, postcentral gyrus; PrcG, precentral gyrus; SF, Sylvian fissure; STG, superior temporal gyrus; STP, supratemporal plane.

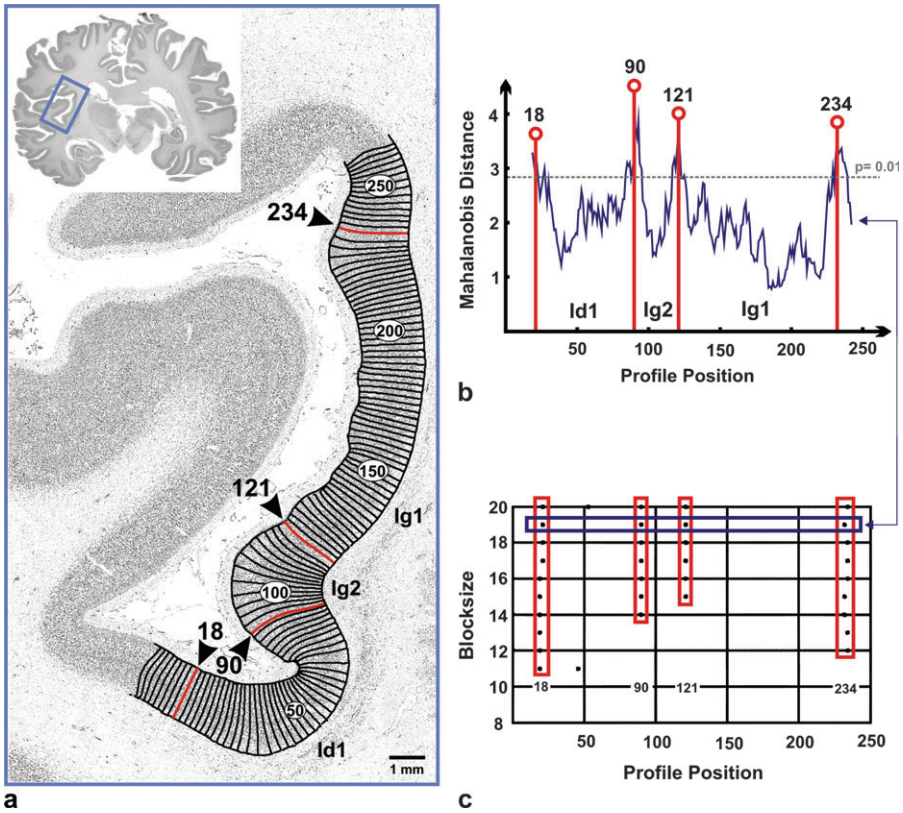

Figure 4. Algorithm-based identification of cortical borders. (*a*) Curvilinear traverses were computed perpendicular to the cortical layers in the insular cortex. Along those traverses, GLI profiles were extracted for the detection of cortical borders (marked in red, see *b* and *c*). (*b*) Mahalanobis distances between adjacent blocks of GLI profiles were calculated (block size = 19). Significant maxima were detected at positions 18, 90, 121, and 234. (*c*) The maxima were found at the same positions even if different block sizes ($8 \leq b \leq 20$; block size 19 marked in blue) were used. Only those maxima were accepted as areal borders, which showed the maxima of the Mahalanobis distances for different block sizes (marked in red, compare *a*–*c*) at the same position.

blockface images containing a reference grid to establish the integrity of the data set orthogonal to the cutting plane, and (iii) digitized images of the highly deformed cell body–stained sections. The defined areas were then interactively transferred to the respective sections of the reconstructed volume. The reconstructed brains were normalized to the stereotactic space of the Montreal Neurological Institute (MNI) single-subject template using a combination of affine transformations and nonlinear elastic registration (Hoemke 2006). To maintain the anterior commissure as the anatomical reference of the coordinate system as described in previous cytoarchitectonic studies (e.g. Amunts et al. 2005; Eickhoff, Schleicher, et al. 2006; Malikovic et al. 2007; Rottschy et al. 2007), the data were shifted by 4 mm (*y*-axis) and 5 mm (*z*-axis) to "anatomical MNI space" (Amunts et al. 2005). Following spatial normalization, the corresponding areas of the different subjects were superimposed and a probabilistic map was generated for each area (Zilles et al. 2002). This map describes for each voxel of the reference brain how many individual brains overlapped with the respective cytoarchitectonic area in that particular voxel (Eickhoff, Paus, et al. 2007).

A maximum probability map (MPM) of these probabilistic maps, that is, a summary map of all defined areas, was then computed by comparing the probabilities for each area (i.e. the numbers of overlapping representations) in each voxel (Eickhoff et al. 2005a) and assigning each voxel to the most likely anatomical area. If different areas showed equally high probabilities for occurring in the same voxel, this voxel was assigned to that area which showed the higher average probability in the 26 directly adjacent voxels.

Results

Using the observer-independent approach for the definition of cortical borders, we identified 3 cytoarchitectonically distinct areas in the posterior insular cortex. Two of these featured a well-developed inner granular layer (layer IV) and may hence be classified as "granular" following the concept of Mesulam and Mufson (1985). In the third area, layer IV was thin and less distinct due to intermingling pyramidal cells from lower layer III, rendering it dysgranular. The 2 granular areas will be referred to as Ig1 and Ig2 ("I" for "insular lobe," "g" for granular areas, and a consecutive dorsal-to-frontal numbering) and the dysgranular one as Id1 ("d" for dysgranular area).

Cytoarchitecture

Ig1 is a granular area characterized by a well-developed and clearly demarcated layer IV as indicated by a corresponding peak in the GLI profile (see Fig. 5*a*). The cortex of Ig1 is thick with wider supragranular than infragranular layers and consists predominantly of small cells with high packing density. Layer II is broad and its border to layer III is blurred. Layer III in turn is made up of numerous small and densely packed pyramidal cells without conspicuous subdivisions or size and density gradients, respectively. Following the well-demarcated inner granular layer IV, layer V contains mainly loosely packed smaller cells. It is followed by layer VI that features no conspicuous increase in cell density as compared with layer V. The white matter border is relatively sharp. This laminar pattern was quantified by the corresponding GLI profile showing a rather homogenous GLI with a single distinct peak corresponding to the granular layer IV.

Area Ig2 can also be characterized as granular based on its wide and clearly distinguishable layer IV (see Fig. 5*b*).

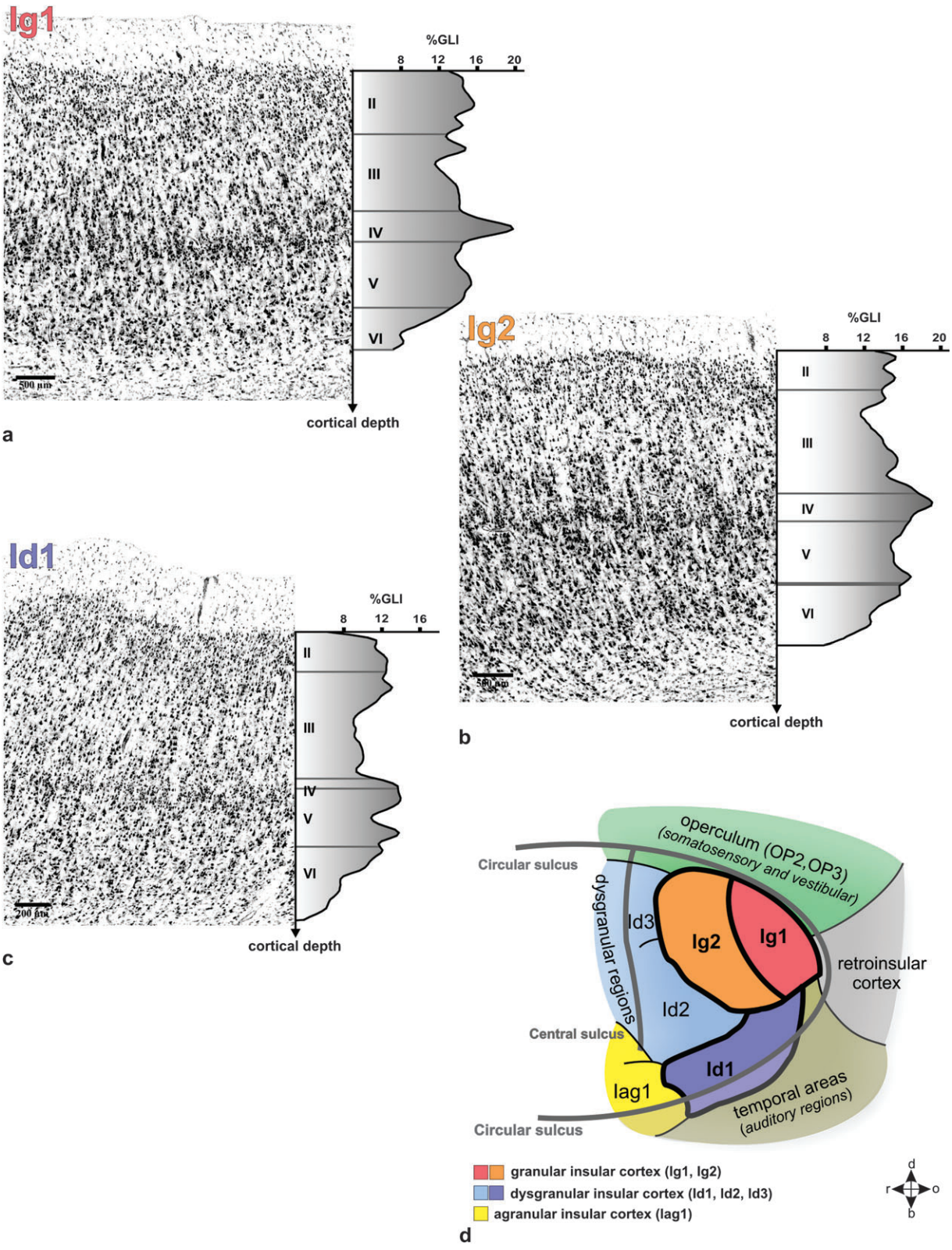

Figure 5. (*a*) Cytoarchitecture of area Ig1. This granular insular area is characterized by a well-developed layer IV, which is reflected by the corresponding peak in the GLI profile. A broad layer II and a less distinct layer V distinguish Ig1 from adjacent areas. (*b*) Cytoarchitecture of area Ig2, which also shows a clearly visible layer IV. Ig2 differs from Ig1 by a smaller layer II, a less cell-dense middle part of layer III, and a cell-denser layer V. (*c*) Cytoarchitecture of area Id1. Layer IV is invaded by pyramidal cells from adjacent layers III and V. This area has, therefore, a dysgranular architecture. Additionally, a less cell-dense layer III distinguishes Id1 from neighboring areas. (*d*) The flatmap shows the posterior insula, which consists of 2 granular areas Ig1 and Ig2. Both areas are adjacent to the more rostral dysgranular region Id1.

Following a relatively densely packed layer II, layer III shows a distinct subdivision into a relatively cell sparse upper part (IIIa + b) and a lower part (IIIc) featuring more prominent pyramidal cells. The inner granular layer (IV) is well developed and clearly discernable from the adjacent pyramidal cell layers. The infragranular layers generally show a higher cell packing density as compared with the supragranular ones. Layer V contains medium-sized and densely packed pyramidal cells. The transition between layer VI and the white matter is blurred by radiating cell columns. The architectonic features of area Ig2 are well reflected by the GLI profile featuring a higher volume fraction of cell bodies in the infragranular layers, a conspicuous sublamination of layer III, and a distinct peak corresponding to layer IV.

Area Id1 features a lower overall cell density as compared with the previously described areas and also shows a considerably less distinctly developed layer IV characterizing it as dysgranular (see Fig. 5*c*). As in Ig2, the cell density is higher in the infragranular part. Layer II is broad, loosely packed with small granular cells, and forms an inconspicuous border to layer III, which homogenously contains loosely packed smaller cells. Layer IV is, in contrast to Ig1 and Ig2, small, cell sparse, and shows intermingling pyramidal cells from lower layer III and upper layer V. However, because it is nevertheless clearly present, Id1 fulfills the criteria of a dysgranular area. Layer V consists of larger, more densely packed pyramidal cells as compared with layer III and can hardly be distinguished from the adjacent layer VI which in turn trails off gradually into the white matter. The GLI profile reflects the lower cell density of this area—in particular its supragranular layers—and confirms the less prominent appearance of layer IV compared with the granular areas.

Macroanatomic Location and Cytoarchitectonic Borders

Both granular areas (Ig1 and Ig2) are located in the dorsal part of the posterior insula and are bordered ventrally and anterior by dysgranular insular cortex as summarized by the schematic flat map provided in Figure 5*d*. All cortical borders were tested for statistically significant changes of cytoarchitectonic features using the Mahalanobis distance measure. We accepted only significant maxima of the distance function as borders. Those borders are characterized by well-localized changes in cytoarchitecture, which can also be seen at low magnification in the microscope, and are reflected by the corresponding peaks of the Mahalanobis distance function (see Fig. 6). We did not observe gradual changes in cytoarchitecture between the mapped areas.

Area Ig1 is located in the dorsal part of the posterior long gyrus, close to posterior end of the circular sulcus where it borders the retroinsular cortex (see Fig. 7). It also has a common border with parietal opercular area OP2 (see Eickhoff, Schleicher, et al. 2006), which commonly extends onto the dorsal part of insula and covers the superior circular sulcus in all

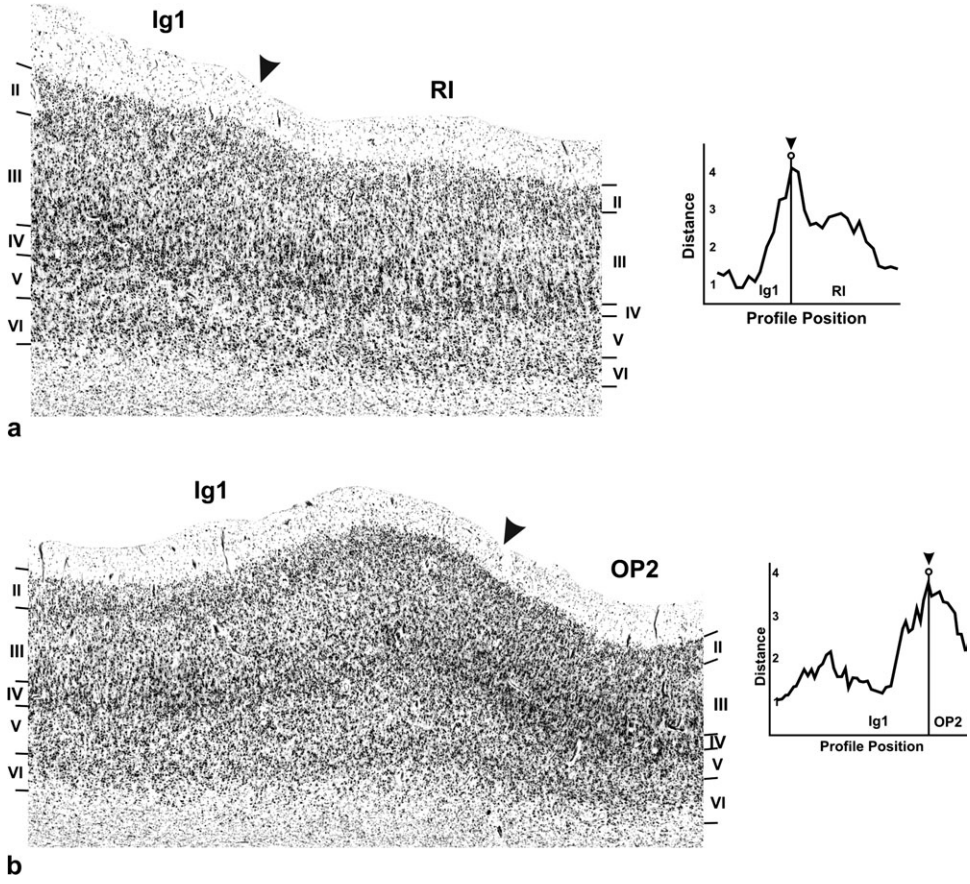

Figure 6. Borders between granular insular area Ig1 and the retroinsular cortex RI (*a*), as well as the parietal opercular area OP2 (*b*). RI differs from Ig1 by a lower cell density in layers III and V and more prominent pyramidal cells in layer IIIc. The border between Ig1 and the opercular area OP2 is characterized by a decrease in cortical thickness and an overall increase in cell density in OP2.

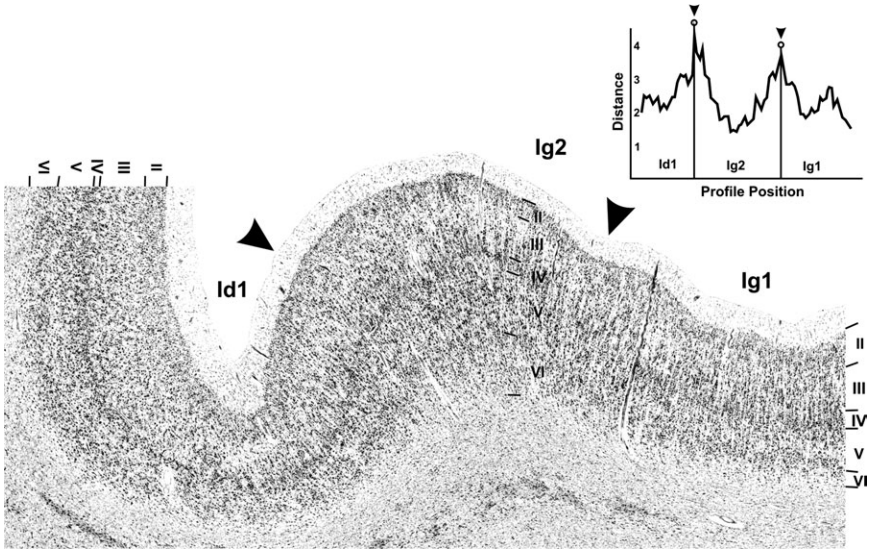

Figure 7. Borders between the insular areas Ig1, Ig2, and Id1. The border between Ig1 and Ig2 is characterized by an increase in cell density particularly in the infragranular layers of Ig2. In Ig2, prominent pyramidal cells in layer IIIc become visible, and the width of layer II decreases. The border between Ig2 and Id1 is characterized by a considerably smaller and less conspicuous layer IV in Id1.

10 brains. Ig1 is followed ventrally by the dysgranular area Id1 and the temporal cortex and rostrally by area Ig2.

The dorsal border of area Ig2 is formed by the opercular areas OP2 and OP3 (Eickhoff, Schleicher, et al. 2006; cf., Fig. 8). It covers the dorsal part of the postcentral insular sulcus and extends onto the postcentral gyrus but does not reach the central sulcus of the insula. Ig2 is followed by area Id1 on its temporal and 2 other dysgranular insular areas on its rostral border (putative areas Id2 and Id3, see Fig. 8). Area Id1, finally, is located mainly around the posterior part of the inferior circular sulcus covering the posterior temporal insula. It extends onto the supratemporal plane though it never reaches Heschl's gyrus. On the supratemporal plane it neighbors the temporoinsular cortex (see Fig. 9). Dorsally, Id1 is neighbored by Ig1 and Ig2, as well as the putative area Id2. The rostral border is formed by an agranular area (see Fig. 9).

Intersubject Architectonic Variability and Volumetric Analysis

We extracted cytoarchitectonic profiles from Ig1, Ig2, Id1, and the adjacent agranular area Iag1 to investigate 1) if our classification into "granular," "dysgranular," and "agranular" is confirmed by quantitative analysis and 2) to test for interindividual, interareal, and gender differences. For investigating the relation between the areas, we applied a cluster analysis, which supported the proposed classification based on the granularity criterion: The analysis revealed 2 clusters based on the RMSSTD index (Sharma 1995). It was found that the granular areas lg1 and lg2 were separated from the dysgranular area (see Fig. 10). The intercluster Euclidean distance was 4.5 in the granular and 6.0 in the other cluster. The intercluster distance was 8.20. The additional assessment of architectonic differences by ANOVA revealed no effect of the putative confounding variables age, gender, and side on the dependent variables. However, the interareal differences were significant ($P < 0.01$) confirming that interareal differences can be established in spite of the marked interindividual variability in cytoarchitecture. The areal volumes calculated from the histological sections (see Table 2), which we tested in a separate ANOVA, showed significant size differences between subjects ($f9_{41} = 5.5$; $P = 0.0001$) indicating a difference in individual brain size. Moreover, they showed significant size differences between the areas ($f2_{41} = 5.26$; $P = 0.0093$) reflecting different areal sizes. All other effects as of sides ($f1_{41} = 0.09$; $P = 0.77$), interaction between area and side ($f2_{41} = 0.06$; $P = 0.94$), interaction between gender and area ($f2_{41} = 1.25$; $P = 0.3$), and interactions between gender, area, and side ($f2_{41} = 0.13$; $P = 0.88$) were not significant.

Probability Maps and MPMs

Probability maps were calculated for each area by superimposing the spatially normalized representations from the different subjects. These maps reflect the probability of observing a particular area at a specific location within the MNI space (see Fig. 11) based on our sample of 10 subjects. They describe the location, spatial extent, and interindividual variability for each area in a standard reference system. Upon examination of these probabilistic maps, it becomes evident that high probabilities for the location of a specific area were observed for 49–140 voxels (for an overlap of 9 of 10 brains). Therefore, interindividual variability was low in comparison to other cytoarchitectonic areas (Choi et al. 2006), especially as the posterior insular areas are relatively small (which aggravates the effects of variability). At lower probabilities, the probabilistic maps of Ig1, Ig2, Id1, and adjacent areas overlapped. A probability of 10% for a certain area at one specific voxel indicates a probability of 90% for another area at this location and vice versa. To assign the most likely area to every voxel, an MPM of the posterior insula was computed.

This MPM represents a contiguous, nonoverlapping parceling of this region (Fig. 12). It hence bears a close resemblance to classical brain maps. Importantly, however, the MPM does not show the parceling of an exemplary or "typical" hemisphere as do previous architectonic brain maps (e.g. Brodmann 1909) but reflects the most likely area at each position in a sample of 10 postmortem brains. This map again illustrates that all areas are located posterior to the central sulcus of the insula and shows

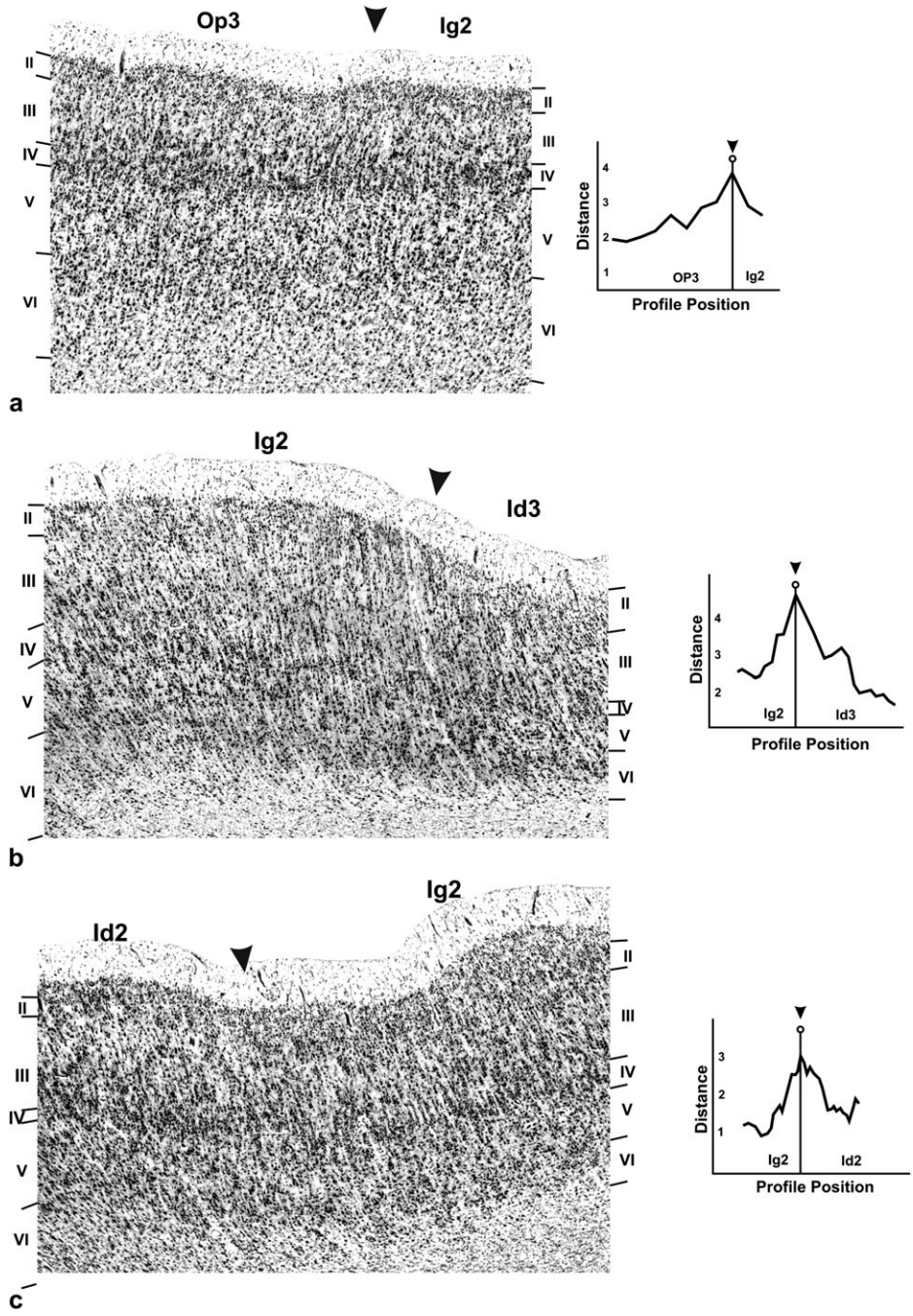

Figure 8. Borders between Ig2 and opercular area OP3 (*a*), Ig2 and an adjacent more dorsal dysgranular insular area Id3 (*b*), as well as Ig2 and an adjacent more ventral dysgranular insular area Id2 (*c*). (*a*) The border between Ig2 and OP3 is characterized by larger and more numerous pyramidal cells in layer V of Ig2. (*b*) The border between Ig2 and Id3 is demarcated by a decrease of cortical thickness and a decrease of layer IV in the dysgranular area Id3. (*c*) The border between Ig2 and Id2 is characterized by a decrease of cell density in layer III and a less conspicuous layer IV in Id2.

that areas Ig1 and Ig2 do not reach the superior circular sulcus. A comparison between the centers of gravity of the MPMs and those of the individual brains revealed a good stereotactic representation as all but one coordinate were located within only one SD. The respective coordinates are given in Table 3.

Discussion

In this study, we reported the architectonic characteristics and stereotaxic location of 3 cytoarchitectonic areas in the posterior human insula as delineated by classical histological criteria and a quantitative analysis (Schleicher et al. 2005). This approach represents a considerable advancement over classical histological studies (Brodmann 1909; von Economo and Koskinas 1925; Bailey and von Bonin 1951) that relied purely on visual inspection of a small sample of postmortem brains. Based on our quantitative analysis, we could refine the classical tripartition of the insular cortex into a granular, a dysgranular, and an agranular part by identifying 2 granular (Ig1 and Ig2) and 1 dysgranular (Id1) area in the posterior insula alone.

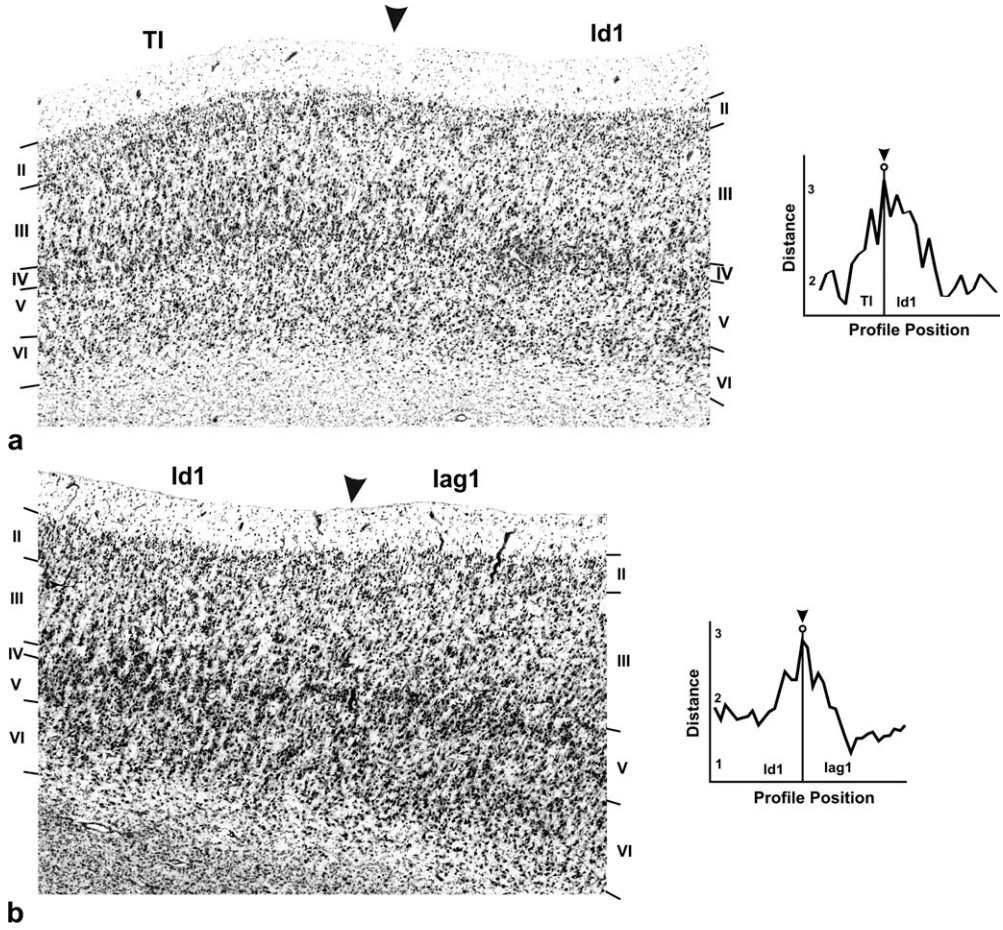

Figure 9. Borders between Id1 and the temporoinsular region TI (*a*) as well as Id1 and the agranular insular area Iag1 (*b*). (*a*) TI differs from Id1 by a higher cell density in layer III of TI. (*b*) The border between Id1 and Iag1 is characterized by a loss of layer IV and a lower cell density in layer II of Iag1.

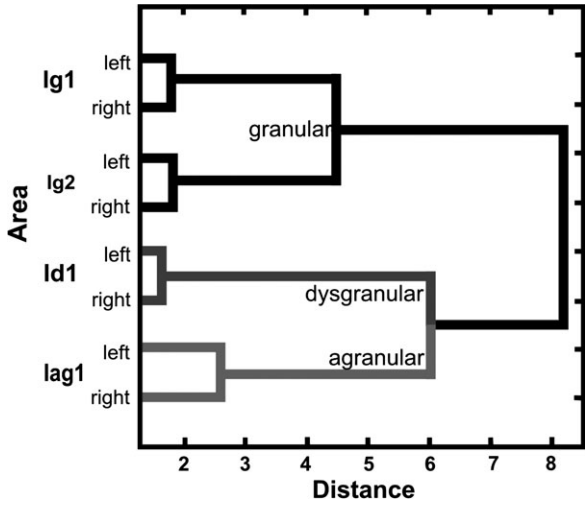

Figure 10. Cluster analysis of mean profiles from areas Ig1, Ig2, Id1, and Iag1. It demonstrates the high differences between areas in contrast to the low distances between sides. The 2 granular areas Ig1 and Ig2 are more similar than the dysgranular and agranular areas.

Table 2
Histological volumes of the areas in a sample of 10 brains

Area	Mean	SD
Id1_l	346.065	107.745
Id1_r	356.274	161.587
Ig1_l	244.422	98.858
Ig1_r	221.155	74.440
Ig2_l	473.193	207.011
Ig2_r	456.364	156.652

Note: All values in cubic millimeters.

It has to be mentioned that the classical tripartition was mainly derived from nonhuman primate studies (Mesulam and Mufson 1982). Although the segregation of the insula in macaques and humans seems to be similar (Mesulam and Mufson 1985), there are still architectonic and macroscopical differences between the species, which become apparent during early development. For example, the presence and course of insular sulci in humans are different from new world monkeys having an entirely smooth insular cortex, as well as from old world monkeys, which only have a single orbitoinsular groove (Shelley and Trimble 2004). Such differences, therefore, make a straightforward extrapolation problematic.

During development, the insular lobe does not grow as fast as the surrounding structures, which form the temporal, parietal, and frontal opercula covering the insula during late fetal stages. At about 13–17 weeks, the limiting sulci start to demarcate and distinguish the insular region from the rest of the cerebral cortex. Between the 20th and 22nd week, the insular sulci begin to demarcate, and at the time of birth, the sulcal pattern

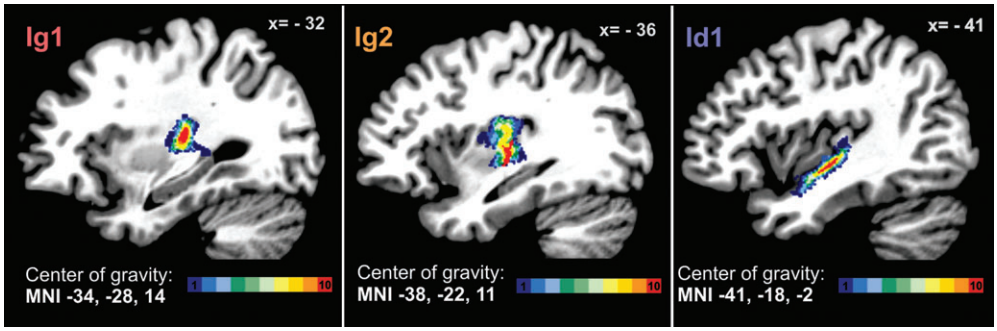

Figure 11. Interindividual variability of Ig1, Ig2, and Id1 in our sample of 10 brains visualized in the MNI single-subject template. The degree of overlap of the areas is color coded (see color bar). The stereotactic *x*-coordinates for the planes are given in the upper right corner. The centers of gravity (see Table 3) are given in the lower left corner.

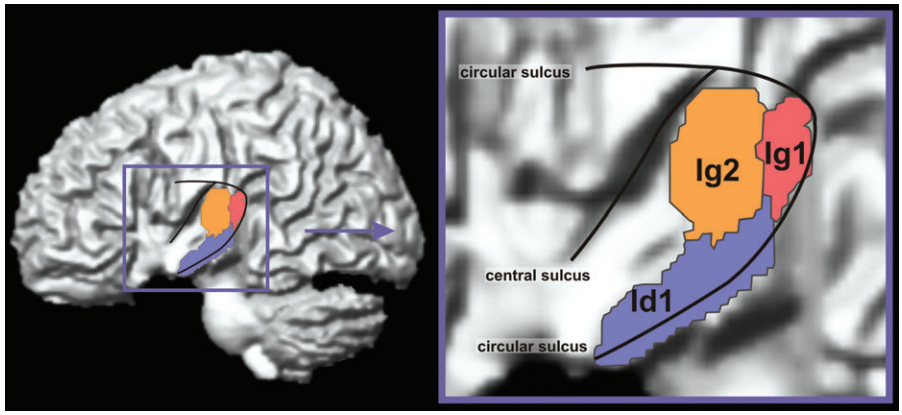

Figure 12. MPM of the posterior insula indicating for each voxel the most likely area. For better visualization, temporal lobe and cortex were removed. The opercular lobe, however, remained.

Table 3
Centers of gravity as well as the minimum overlap used for calculation of the MPMs for each area

Area	Center of gravity in anatomical MNI-space (Amunts et al. 2005)			Overlap MPMs (%)
	x	*y*	*z*	
Ig1 left				
Individuals	−34.6 ± 1.1	−27.6 ± 1.2	14.0 ± 2.7	66
MPM	−33	−29	13	
p-map	−34	−28	14	
Ig1 right				
Individuals	34.5 ± 1.9	−26.5 ± 1.3	11.5 ± 3.1	
MPM	34	−27	11	59.50
p-map	35	−27	11	
Ig2 left				
Individuals	−38.0 ± 1.1	−22.0 ± 2.7	11.0 ± 2.6	
MPM	−38	−22	11	60.80
p-map	−38	−22	11	
Ig2 right				
Individuals	37.2 ± 1.9	−21.4 ± 1.7	10.2 ± 2.8	
MPM	38	−20	11	54.60
p-map	38	−21	10	
Id1 left				
Individuals	−41.4 ± 1.9	−18.1 ± 3.5	−2.6 ± 2.7	
MPM	−41	−18	−3	58.90
p-map	−41	−18	−2	
Id1 right				
Individuals	40.6 ± 1.3	−16.7 ± 3.8	−5.4 ± 4.2	
MPM	41	−17	−5	56.70
p-map	41	−17	−5	

Note: Coordinates are given for the individual brains as well as for the probability maps and the MPMs.

presents an almost adult appearance (Cunningham 1891; Afif et al. 2007).

Although a multitude of functions has been ascribed to the insula, there is evidence for a functional segregation between at least the anterior and posterior insula. Olfactory, gustatory, and emotional stimuli have been described to elicit activations in the anterior insula (Poellinger et al. 2001; Kringelbach et al. 2004; Small and Prescott 2005; Frith and Singer 2008; Singer and Lamm 2009). This is in accordance with connectivity studies in nonhuman primates that indicate a dense connection between the anterior insula and the amygdala, the perirhinal and the entorhinal cortex, and parts of the prefrontal lobe (Mesulam and Mufson 1985; Augustine 1996). In contrast, the posterior insula seems to be connected to primary and secondary somatosensory areas and the supplementary motor area (SMA). In humans, these areas have been found to be involved in sensorimotor tasks.

Previous Cytoarchitectonic Maps

Earlier maps divided the insular cortex into a granular posterior and an agranular anterior part (Brodmann 1909) or additionally introduced a precentral dysgranular region (von Economo and Koskinas 1925). One map (Bailey and von Bonin 1951) is particularly interesting as it distinguishes 3 individual areas in the human insula while at the same time both parietal and temporal lobe were conceptualized as a homogenous region.

Upon closer inspection, however, it becomes apparent that they labeled the posterior insula as a continuation of parietal and temporal regions. A very detailed map (Rose 1928) reports multiple areas in the human insula distinguished primarily by their granularity. A synopsis of these classical brain maps clearly shows that all authors separated the human insula into a granular posterior and an agranular anterior region. The additional delineation of an intermediate dysgranular part, as well as the exact location of the borders between these regions, however, varies widely between different maps.

In more recent maps, which describe the insula of nonhuman primates (Mesulam and Mufson 1982) and subsequently of man (Mesulam and Mufson 1985), the concept of granularity was explicitly introduced to subdivide the insular lobe into 3 belt-like regions. In both humans and nonhuman primates, a circular organization of the insular cortex surrounding its allocortical pole was proposed. The inner agranular belt is surrounded by a dysgranular zone, which is then followed by a granular part covering the dorsal posterior insula. This map hence not only corresponds to classical mapping approaches by describing a granular posterior insula and—in accordance to a highly detailed map (Rose 1928)—a posterior–ventral dysgranular region but also additionally pinpoints the main criterion used by previous examiners introducing the concept of belts of different degrees of granularity.

Our own data on the cytoarchitecture of the human posterior insula are in accordance with classical maps. It demonstrates the existence of granular cortical areas in the posterior–dorsal insula. Moreover, according to detailed earlier maps (Rose 1928; Mesulam and Mufson 1985), we could identify a dysgranular cortex adjoining the granular zone on its anterior and ventral border. Beyond these commonalities, the cytoarchitectonic map presented here enlarges the current view of the human insula as it demonstrates the presence of several distinct subregions within the granular and dysgranular zones. These subdivisions of the granular and dysgranular region may have important implications for understanding the role of the human insula as it can be expected that different cytoarchitectonic entities also sustain different functional capacities. The here-described feature of granularity is the most conspicuous and regularly reported difference between insular areas.

Functional Roles of the Posterior Insula

Activations in the insula have been reported for virtually all cognitive, affective, and sensory paradigms tested in functional imaging studies and have also been implicated by research in nonhuman primates. However, the most reliable evidence of an involvement of the posterior insula has been received for studies investigating painful, somatosensory, auditory, and interoceptive stimuli, as well as motor paradigms. For these functions, a variety of functional imaging, electrophysiological, and connectivity studies are available in humans and nonhuman primates. We will therefore focus on these functions and their relationship to the posterior insula.

Activation by Somatosensory Stimuli

In nonhuman primates, the posterior insula was shown to have direct connections to somatosensory areas and was thus assigned to be a higher level component of the somatosensory system (Mesulam and Mufson 1985; Friedman et al. 1986; Augustine 1996). In particular, this region was reported to be reciprocally connected with the neighboring secondary somatosensory cortex (SII) and to receive projections from the primary somatosensory cortex (in particular areas 3b, 1, and 2) and somatosensory association areas 5 (PE) and 7b (PF) (Mufson and Mesulam 1982; Mesulam and Mufson 1985; Friedman et al. 1986). Efferents were described to reach amygdala, frontal cortex, perirhinal cortex, and hippocampus (Friedman et al. 1986; Augustine 1996). Along with these findings, this region was interpreted to play a role in tactile memory or emotion-related processing (Mesulam and Mufson 1985; Augustine 1996; Dijkerman and de Haan 2007).

Single-unit recording studies in monkeys consequently reported responses to somatosensory activation in the dorsal posterior insula (Robinson and Burton 1980; Schneider et al. 1993; Zhang et al. 1999; Coq et al. 2004). However, not a mere somatosensory representation but rather multisensory processing was observed as different recording sites responded to auditory, baroreceptive, or painful stimuli (Zhang et al. 1999; Coq et al. 2004). The recordings thus did not only support the theory of the posterior insula as a somatosensory association region but also indicated that it might play a more multisensory and hence most likely integrative role.

In humans, somatosensory activation of the posterior insular cortex was shown by direct intracerebral stimulation in patients undergoing surgery for temporal lobe epilepsy (Ostrowsky et al. 2002), as well as by functional imaging studies. These studies investigated simple stimulation paradigms, as well as more complex tasks like rating the roughness of gratings or tactile object recognition (Gelnar et al. 1998; Deuchert et al. 2002; Reed et al. 2004; Kitada et al. 2005). Regarding the results from connectivity and single-cell studies, these results corroborate a role of the posterior insula in somatosensory processing.

Activation by Pain

Connectivity studies in monkeys reported the posterior insula to be a part of the pain network consisting of the primary and secondary somatosensory areas, anterior cingulate cortex, prefrontal cortex, and the amygdala (for review, see Peyron et al. 2000; Chen 2007). In particular, afferent connections were reported to reach the insula from primary and secondary somatosensory cortices (Friedman et al. 1986; Augustine 1996), as well as from pain-specific parts of the thalamus (Craig et al. 1994). Efferents were reported to reach amygdala and prefrontal cortex (Mesulam and Mufson 1985; Augustine 1996), as well as the cingulum (Mesulam and Mufson 1985). In line with these findings, functional recordings in monkeys directly demonstrated the involvement of the insular cortex in pain processing (Baumgärtner et al. 1998). This study demonstrated that laser-evoked noxious potentials could be recorded from the posterior insular cortex in anesthetized monkeys. Extracellular single-unit recordings (Zhang et al. 1999) reported responses to painful stimuli in the middle and anterior insula close to touch and baroreceptive responsive units. Again, this points to an integrative processing in the insula.

Functional imaging and electrophysiological studies in humans also have repeatedly demonstrated the responsiveness of the insula to painful stimulation (Peyron et al. 2000, 2002; Treede et al. 2000; Frot and Mauguiere 2003; Alkire et al. 2004; Brooks et al. 2005; Chen 2007). However, the exact location of pain-related activity in the insular cortex varies between studies as some authors report a focus of activation posterior (Craig et al. 1994; Alkire et al. 2004), whereas others describe it

rather in the mid-insula (Treede et al. 2000; Peyron et al. 2002; Brooks et al. 2005; Chen 2007) in addition to a well-established operculoinsular activation site (Peyron et al. 2000; Chen 2007). Due to the close spatial proximity in this region, a relation of this site to a defined anatomic structure is difficult (Farrell et al. 2005). However, as well for the opercular region OP1 (Frot et al. 2001; Eickhoff, Amunts, et al. 2006) as for the posterior insula (Frot et al. 2007), a role in pain processing has already been demonstrated. Further investigation in this region will therefore require a careful differentiation of insular and opercular activations, as previously demonstrated by fMRI (Alkire et al. 2004) and electrophysiological methods (Frot and Mauguiere 2003; Frot et al. 2007). This is even more important as the above-discussed posterior insular activation in somatosensory paradigms seems to contradict a described non-somatosensory role in pain intensity rating (Frot et al. 2007). The cytoarchitectonic maps presented here may provide an effective means for addressing these issues by enabling a direct comparison of somatosensory and painful stimuli, respectively, with the differentiated cytoarchitectonic organization of opercular and insular areas.

Motor Activation

Connections between the posterior insula and the frontal motor areas have also been demonstrated in nonhuman primates. In particular, invasive tracing techniques revealed projections of the granular insula toward SMA proper and afferent connections reaching the dysgranular insula from the pre-SMA (Luppino et al. 1993; Augustine 1996).

Those findings are in accordance with the observation that movement may be elicited by electrical stimulation of the posterior insula in humans (Showers and Lauer 1961), which also underlines the functional relevance of these connections to movement production. Functional imaging studies revealed increased motor activation during the attention condition in the posterior insular cortex (Johansen-Berg and Matthews 2002), as well as a role in sensorimotor integration (Ciccarelli et al. 2005). With regard to a discussed role of this region in sensory learning (Mesulam and Mufson 1985; Augustine 1996; Dijkerman and de Haan 2007), it might relay relevant sensory feedback to motor areas. This would be in accordance with different studies in patients, which showed role of this region in motor recovery after stroke in humans (Chollet et al. 1991; Carey et al. 2005; Loubinoux et al. 2007).

Activation by Interoception

Studies in monkey brains report insular connections to the hypothalamus (Mesulam and Mufson 1985; Craig 2002) and to thalamic nuclei that are known to relay information from the autonomic nervous system. It was suggested that these connections indicate a role of the insula in interoception (Craig 2002). Single-cell studies in macaques support this hypothesis because responses (slightly lateralized to the right) to changes in blood pressure were recorded (Zhang et al. 1999). Interestingly, right insular strokes result in a higher risk of cardiac complications (Colivicchi et al. 2004). A sympathetic dominance in the right and parasympathetic dominance in the left insula have been reported (Oppenheimer 2006).

Functional imaging studies describe insular activation in breath holding (McKay et al. 2008), viscerosensory processing (Aziz et al. 2000), as well as a role in cardiovascular regulation (Oppenheimer 2006). In epileptic patients, insular seizures show both visceral and respiratory manifestations (Guenot and Isnard 2008). However, as baroreceptive response units in monkeys were found in the mid-insula rather than the posterior insula (Zhang et al. 1999), interoception is probably a function for more anterior parts of the insula and not for the posterior part mapped in the present observations.

Auditory Activation

Connectivity studies in monkeys implicate an involvement of the posterior insula in auditory processing. Direct connections from the medial geniculate body were reported to reach the granular and to a lesser extent also the dysgranular insular regions (Burton and Jones 1976). Furthermore, direct connections between posterior insula and auditory cortex were described (Mesulam and Mufson 1985; Smiley et al. 2007). Single-cell recordings in monkeys go well with these findings as they revealed that posterior insular neurons responded directly to auditory stimuli (Bieser and Muller-Preuss 1996; Bieser 1998), though a close spatial proximity to somatosensory stimuli was described (Coq et al. 2004).

These results are corresponding to reports that show the human insula to be involved "in several key auditory processes" (for review, see Bamiou et al. 2003) and hypothesized it to participate in sensory as well as integrating aspects of auditory processing. Summed up, a more integrative function in this area can be assumed for auditory functions as well. However, the degree of integration and differentiation of functions has still to be investigated.

Conclusions

Using an observer-independent approach, we could identify 3 distinct cytoarchitectonic areas in the human posterior insula. Although this new scheme does not contradict previous classification of the insular cortex based on its granularity, it further develops these maps by demonstrating the existence of several individual areas within these major zones. Given the variety of functions ascribed to the (posterior) insula based on functional imaging studies and investigations of connectivity, it seems reasonable that these subdivisions form the anatomical substrate of a diversified mosaic of structurally and functionally distinct areas in the human posterior insula. As probabilistic maps of each area have been computed in standard MNI space, this hypothesis can now be rigorously tested by comparing anatomical and functional data. This was not possible on the basis of the previous schematic maps. Such integration of structural and functional information will allow a further characterization of the segregation and integration of different modalities (Zilles and Amunts 2009) within this region. To support the usage of our anatomical data for this purpose, the probabilistic cytoarchitectonic maps of areas Ig1, Ig2, and Id1 including a software for integrating the maps into the widely used software package SPM, FSL, and AFNI is available at http://www.fz-juelich.de/ime/spm_anatomy_toolbox.

Funding

Human Brain Project/Neuroinformatics research by the National Institute of Biomedical Imaging and Bioengineering; National Institute of Neurological Disorders and Stroke; National Institute of Mental Health; Helmholtz Alliance "Systems Biology" the "Human Brain Model" (WP02 P03 to K.Z. and S.E.).

Notes

Conflict of Interest: None declared.

Address correspondence to Florian Kurth, Institute for Neurosciences and Medicine (INM-2), Forschungszentrum Jülich GmbH, Leo-Brandt Strasse 5, 52425 Jülich, Germany. Email: f.kurth@fz-juelich.de.

References

Afif A, Bouvier R, Buenerd A, Trouillas J, Mertens P. 2007. Development of the human fetal insular cortex: study of the gyration from 13 to 28 gestational weeks. Brain Struct Funct. 212:335–346.

Alkire MT, White NS, Hsieh R, Haier RJ. 2004. Dissociable brain activation responses to 5-Hz electrical pain stimulation: a high-field functional magnetic resonance imaging study. Anesthesiology. 100:939–946.

Amunts K, Kedo O, Kindler M, Pieperhoff P, Mohlberg H, Shah NJ, Habel U, Schneider F, Zilles K. 2005. Cytoarchitectonic mapping of the human amygdala, hippocampal region and entorhinal cortex: intersubject variability and probability maps. Anat Embryol (Berl). 210:343–352.

Amunts K, Schleicher A, Zilles K. 2007. Cytoarchitecture of the cerebral cortex—more than localization. Neuroimage. 37:1061–1065.

Amunts K, Weiss PH, Mohlberg H, Pieperhoff P, Eickhoff S, Gurd JM, Marshall JC, Shah NJ, Fink GR, Zilles K. 2004. Analysis of neural mechanisms underlying verbal fluency in cytoarchitectonically defined stereotaxic space—the roles of Brodmann areas 44 and 45. Neuroimage. 22:42–56.

Annett M. 1973. Handedness in families. Ann Hum Genet. 37:93–105.

Augustine JR. 1996. Circuitry and functional aspects of the insular lobe in primates including humans. Brain Res Brain Res Rev. 22:229–244.

Aziz Q, Thompson DG, Ng VWK, Hamdy S, Sarkar S, Brammer MJ, Bullmore ET, Hobson A, Tracey I, Gregory L, et al. 2000. Cortical processing of human somatic and visceral sensation. J Neurosci. 20:2657–2663.

Bailey P, von Bonin G. 1951. The isocortex of man. Urbana (IL): University of Illinois Press.

Bamiou DE, Musiek FE, Luxon LM. 2003. The insula (Island of Reil) and its role in auditory processing. Literature review. Brain Res Brain Res Rev. 42:143–154.

Baumgärtner U, Tiede W, Treede RD, Craig AD. 2006. Laser-evoked potentials are graded and somatotopically organized anteroposteriorly in the operculoinsular cortex of anesthetized monkeys. J Neurophysiol. 96:2802–2808.

Baumgärtner U, Vogel H, Ellrich J, Gawehn J, Stoeter P, Treede RD. 1998. Brain electrical source analysis of primary cortical components of the tibial nerve somatosensory evoked potential using regional sources. Electroencephalogr Clin Neurophysiol. 108:588–599.

Bieser A. 1998. Processing of twitter-call fundamental frequencies in insula and auditory cortex of squirrel monkeys. Exp Brain Res. 122:139–148.

Bieser A, Muller-Preuss P. 1996. Auditory responsive cortex in the squirrel monkey: neural responses to amplitude-modulated sounds. Exp Brain Res. 108:273–284.

Brodmann K. 1909. Vergleichende Lokalisationslehre der Großhirnrinde in ihren Prinzipien dargestellt auf Grund des Zellenbaues. Leipzig (Germany): Barth J.A.

Brooks JC, Zambreanu L, Godinez A, Craig AD, Tracey I. 2005. Somatotopic organisation of the human insula to painful heat studied with high resolution functional imaging. Neuroimage. 27:201–209.

Burton H, Jones EG. 1976. The posterior thalamic region and its cortical projection in new world and old world monkeys. J Comp Neurol. 168:249–301.

Carey LM, Abbott DF, Egan GF, Bernhardt J, Donnan GA. 2005. Motor impairment and recovery in the upper limb after stroke: behavioral and neuroanatomical correlates. Stroke. 36:625–629.

Chen LM. 2007. Imaging of pain. Int Anesthesiol Clin. 45:39–57.

Choi HJ, Zilles K, Mohlberg H, Schleicher A, Fink GR, Armstrong E, Amunts K. 2006. Cytoarchitectonic identification and probabilistic mapping of two distinct areas within the anterior ventral bank of the human intraparietal sulcus. J Comp Neurol. 495:53–69.

Chollet F, DiPiero V, Wise RJ, Brooks DJ, Dolan RJ, Frackowiak RS. 1991. The functional anatomy of motor recovery after stroke in humans: a study with positron emission tomography. Ann Neurol. 29:63–71.

Ciccarelli O, Toosy AT, Marsden JF, Wheeler-Kingshott CM, Sahyoun C, Matthews PM, Miller DH, Thompson AJ. 2005. Identifying brain regions for integrative sensorimotor processing with ankle movements. Exp Brain Res. 166:31–42.

Colivicchi F, Bassi A, Santini M, Caltagirone C. 2004. Cardiac autonomic derangement and arrhythmias in right-sided stroke with insular involvement. Stroke. 35:2094–2098.

Coq JO, Qi H, Collins CE, Kaas JH. 2004. Anatomical and functional organization of somatosensory areas of the lateral fissure of the new world titi monkey (*Callicebus moloch*). J Comp Neurol. 476: 363–387.

Craig AD. 2002. How do you feel? Interoception: the sense of the physiological condition of the body. Nat Rev Neurosci. 3:655–666.

Craig AD, Bushnell MC, Zhang ET, Blomqvist A. 1994. A thalamic nucleus specific for pain and temperature sensation. Nature. 372:770–773.

Craig AD, Chen K, Bandy D, Reiman EM. 2000. Thermosensory activation of insular cortex. Nat Neurosci. 3:184–190.

Cunningham DJ. 1891. Development of the gyri and sulci on the surface of the Island of Reil of the human brain. J Anat Physiol. 25:338–348.

Deuchert M, Ruben J, Schwiemann J, Meyer R, Thees S, Krause T, Blankenburg F, Villringer K, Kurth R, Curio G, et al. 2002. Event-related fMRI of the somatosensory system using electrical finger stimulation. Neuroreport. 13:365–369.

Dijkerman HC, de Haan EH. 2007. Somatosensory processes subserving perception and action. Behav Brain Sci. 30:189–201.

Dixon WJ, Brown MB, Engelman L, Hill MA, Jennrich RI. 1988. BMDP Statistical Software Manual. Berkley: University of California Press.

Dombrowski SM, Hilgetag CC, Barbas H. 2001. Quantitative architecture distinguishes prefrontal cortical systems in the rhesus monkey. Cereb Cortex. 11:975–988.

Eickhoff SB, Amunts K, Mohlberg H, Zilles K. 2006. The human parietal operculum. II. Stereotaxic maps and correlation with functional imaging results. Cereb Cortex. 16:268–279.

Eickhoff SB, Paus T, Caspers S, Grosbras MH, Evans AC, Zilles K, Amunts K. 2007. Assignment of functional activations to probabilistic cytoarchitectonic areas revisited. Neuroimage. 36:511–521.

Eickhoff SB, Schleicher A, Scheperjans F, Palomero-Gallagher N, Zilles K. 2007. Analysis of neurotransmitter receptor distribution patterns in the cerebral cortex. Neuroimage. 34:1317–1330.

Eickhoff SB, Schleicher A, Zilles K, Amunts K. 2006. The human parietal operculum. I. Cytoarchitectonic mapping of subdivisions. Cereb Cortex. 16:254–267.

Eickhoff SB, Stephan KE, Mohlberg H, Grefkes C, Fink GR, Amunts K, Zilles K. 2005. A new SPM toolbox for combining probabilistic cytoarchitectonic maps and functional imaging data. Neuroimage. 25:1325–1335.

Farrell MJ, Laird AR, Egan GF. 2005. Brain activity associated with painfully hot stimuli applied to the upper limb: a meta-analysis. Hum Brain Mapp. 25:129–139.

Fasold O, von Brevern M, Kuhberg M, Ploner CJ, Villringer A, Lempert T, Wenzel R. 2002. Human vestibular cortex as identified with caloric stimulation in functional magnetic resonance imaging. Neuroimage. 17:1384–1393.

Fink GR, Marshall JC, Weiss PH, Stephan T, Grefkes C, Shah NJ, Zilles K, Dieterich M. 2003. Performing allocentric visuospatial judgments with induced distortion of the egocentric reference frame: an fMRI study with clinical implications. Neuroimage. 20:1505–1517.

Friedman DP, Murray EA, O'Neill JB, Mishkin M. 1986. Cortical connections of the somatosensory fields of the lateral sulcus of macaques: evidence for a corticolimbic pathway for touch. J Comp Neurol. 252:323–347.

Frith CD, Singer T. 2008. The role of social cognition in decision making. Philos Trans R Soc Lond B Biol Sci. 363:3875–3886.

Frot M, Garcia-Larrea L, Guenot M, Mauguiere F. 2001. Responses of the supra-sylvian (SII) cortex in humans to painful and innocuous stimuli—a study using intra-cerebral recordings. Pain. 94:65–73.

Frot M, Magnin M, Mauguiere F, Garcia-Larrea L. 2007. Human SII and posterior insula differently encode thermal laser stimuli. Cereb Cortex. 17:610–620.

Frot M, Mauguiere F. 2003. Dual representation of pain in the operculoinsular cortex in humans. Brain. 126:438–450.

Gelnar PA, Krauss BR, Szeverenyi NM, Apkarian AV. 1998. Fingertip representation in the human somatosensory cortex: an fMRI study. Neuroimage. 7:261–283.
Guenot M, Isnard J. 2008. [Epilepsy and insula]. Neurochirurgie. 54:374–381.
Hoemke L. 2006. A multigrid method for anisotrophic PDE's in elastic image registration. Numer Linear Algebra Appl. 13:215–229.
Hua lH, Strigo IA, Baxter LC, Johnson SC, Craig AD. 2005. Anteroposterior somatotopy of innocuous cooling activation focus in human dorsal posterior insular cortex. Am J Physiol Regul Integr Comp Physiol. 289:R319–R325.
Johansen-Berg H, Matthews PM. 2002. Attention to movement modulates activity in sensori-motor areas, including primary motor cortex. Exp Brain Res. 142:13–24.
Kitada R, Hashimoto T, Kochiyama T, Kito T, Okada T, Matsumura M, Lederman SJ, Sadato N. 2005. Tactile estimation of the roughness of gratings yields a graded response in the human brain: an fMRI study. Neuroimage. 25:90–100.
Kretschmann HJ, Tafesse U, Herrmann A. 1982. Different volume changes of cerebral cortex and white matter during histological preparation. Microsc Acta. 86:13–24.
Kringelbach ML, de Araujo IE, Rolls ET. 2004. Taste-related activity in the human dorsolateral prefrontal cortex. Neuroimage. 21:781–788.
Loubinoux I, Dechaumont-Palacin S, Castel-Lacanal E, De Boissezon X, Marque P, Pariente J, Albucher JF, Berry I, Chollet F. 2007. Prognostic value of FMRI in recovery of hand function in subcortical stroke patients. Cereb Cortex. 17:2980–2987.
Luppino G, Matelli M, Camarda R, Rizzolatti G. 1993. Corticocortical connections of area F3 (SMA-proper) and area F6 (pre-SMA) in the macaque monkey. J Comp Neurol. 338:114–140.
Mahalanobis PC, Majumda DN, Rao DC. 1949. Anthropometric survey of the united provinces. A statistical study. Sankhya. 9:89–324.
Malikovic A, Amunts K, Schleicher A, Mohlberg H, Eickhoff SB, Wilms M, Palomero-Gallagher N, Armstrong E, Zilles K. 2007. Cytoarchitectonic analysis of the human extrastriate cortex in the region of V5/MT+: a probabilistic, stereotaxic map of area hOc5. Cereb Cortex. 17:562–574.
McKay LC, Adams L, Frackowiak RS, Corfield DR. 2008. A bilateral cortico-bulbar network associated with breath holding in humans, determined by functional magnetic resonance imaging. Neuroimage. 40:1824–1832.
Merker B. 1983. Silver staining of cell bodies by means of physical development. J Neurosci Methods. 9:235–241.
Mesulam MM, Mufson EJ. 1982. Insula of the old world monkey. I. Architectonics in the insulo-orbito-temporal component of the paralimbic brain. J Comp Neurol. 212:1–22.
Mesulam MM, Mufson EJ. 1985. The insula of Reil in man and monkey. Architectonics, connectivity and function. In: Peters A, Jones EG, editors. Cerebral cortex. New York: Plenum Press. p. 179–226.
Morgane PJ, Jacobs MS, McFarland WL. 1980. The anatomy of the brain of the bottlenose dolphin (Tursiops truncatus): surface configurations of the telencephalon of the bottlenose dolphin with comparative anatomical observations in four other cetacean species. New York: Ankho International Fayetteville.
Mufson EJ, Mesulam MM. 1982. Insula of the old world monkey. II: afferent cortical input and comments on the claustrum. J Comp Neurol. 212:23–37.
Naidich TP, Kang E, Fatterpekar GM, Delman BN, Gultekin SH, Wolfe D, Ortiz O, Yousry I, Weismann M, Yousry TA. 2004. The insula: anatomic study and MR imaging display at 1.5 T. AJNR Am J Neuroradiol. 25:222–232.
Ono M, Kubik S, Abernathey CD. 1990. Atlas of the cerebral sulci. Stuttgart (Germany): Thieme.
Oppenheimer S. 2006. Cerebrogenic cardiac arrhythmias: cortical lateralization and clinical significance. Clin Auton Res. 16:6–11.
Ostrowsky K, Magnin M, Ryvlin P, Isnard J, Guenot M, Mauguiere F. 2002. Representation of pain and somatic sensation in the human insula: a study of responses to direct electrical cortical stimulation. Cereb Cortex. 12:376–385.
Peyron R, Frot M, Schneider F, Garcia-Larrea L, Mertens P, Barral FG, Sindou M, Laurent B, Mauguiere F. 2002. Role of operculoinsular cortices in human pain processing: converging evidence from PET, fMRI, dipole modeling, and intracerebral recordings of evoked potentials. Neuroimage. 17:1336–1346.
Peyron R, Laurent B, Garcia-Larrea L. 2000. Functional imaging of brain responses to pain. A review and meta-analysis (2000). Neurophysiol Clin. 30:263–288.
Poellinger A, Thomas R, Lio P, Lee A, Makris N, Rosen BR, Kwong KK. 2001. Activation and habituation in olfaction—an fMRI study. Neuroimage. 13:547–560.
Reed CL, Shoham S, Halgren E. 2004. Neural substrates of tactile object recognition: an fMRI study. Hum Brain Mapp. 21:236–246.
Robinson CJ, Burton H. 1980. Organization of somatosensory receptive fields in cortical areas 7b, retroinsula, postauditory and granular insula of M. fascicularis. J Comp Neurol. 192:69–92.
Rose M. 1928. Die Inselrinde des Menschen und der Tiere. J Psychol Neurol. 37:467–624.
Rottschy C, Eickhoff SB, Schleicher A, Mohlberg H, Kujovic M, Zilles K, Amunts K. 2007. Ventral visual cortex in humans: cytoarchitectonic mapping of two extrastriate areas. Hum Brain Mapp. 28:1045–1059.
Schleicher A, Amunts K, Geyer S, Kowalski T, Schormann T, Palomero-Gallagher N, Zilles K. 2000. A stereological approach to human cortical architecture: identification and delineation of cortical areas. J Chem Neuroanat. 20:31–47.
Schleicher A, Palomero-Gallagher N, Morosan P, Eickhoff SB, Kowalski T, de Vos K, Amunts K, Zilles K. 2005. Quantitative architectural analysis: a new approach to cortical mapping. Anat Embryol (Berl). 210:373–386.
Schleicher A, Zilles K. 1990. A quantitative approach to cytoarchitectonics: analysis of structural inhomogeneities in nervous tissue using an image analyser. J Microsc. 157:367–381.
Schneider RJ, Friedman DP, Mishkin M. 1993. A modality-specific somatosensory area within the insula of the rhesus monkey. Brain Res. 621:116–120.
Sharma SC. 1995. Applied multivariate techniques. New York: John Wiley & Sons.
Shelley BP, Trimble MR. 2004. The insular lobe of Reil–its anatamico-functional, behavioural and neuropsychiatric attributes in humans–a review. World J.Biol.Psychiatry. 5:176–200.
Showers MJ, Lauer EW. 1961. Somatovisceral motor patterns in the insula. J Comp Neurol. 117:107–115.
Singer T, Lamm C. 2009. The social neuroscience of empathy. Ann N Y Acad Sci. 1156:81–96.
Small DM, Prescott J. 2005. Odor/taste integration and the perception of flavor. Exp Brain Res. 166:345–357.
Smiley JF, Hackett TA, Ulbert I, Karmas G, Lakatos P, Javitt DC, Schroeder CE. 2007. Multisensory convergence in auditory cortex, I. Cortical connections of the caudal superior temporal plane in macaque monkeys. J Comp Neurol. 502:894–923.
Toga AW, Thompson PM, Mori S, Amunts K, Zilles K. 2006. Towards multimodal atlases of the human brain. Nat Rev Neurosci. 7:952–966.
Treede RD, Apkarian AV, Bromm B, Greenspan JD, Lenz FA. 2000. Cortical representation of pain: functional characterization of nociceptive areas near the lateral sulcus. Pain. 87:113–119.
Vogt C, Vogt O. 1919. Allgemeine Ergebnisse unserer Hirnforschung. J Psychol Neurol. 25:279–1262.
von Economo C, Koskinas GN. 1925. Die Cytoarchitectonik der Hirnrinde des erwachsenen Menschen. Berlin (Germany): Springer Verlag.
Zhang ZH, Dougherty PM, Oppenheimer SM. 1999. Monkey insular cortex neurons respond to baroreceptive and somatosensory convergent inputs. Neuroscience. 94:351–360.
Zilles K. 2004. Architecture of the human cerebral cortex. Regional and laminar organization. In: Paxinos G, editor. The human nervous system. 2nd ed. San Diego (CA): Elsevier. p. 997–1055.
Zilles K, Amunts K. 2009. Receptor mapping: architecture of the human cerebral cortex. Curr Opin Neurol. 22:331–339.
Zilles K, Eickhoff S, Palomero-Gallagher N. 2003. The human parietal cortex: a novel approach to its architectonic mapping. Adv Neurol. 93:1–21.
Zilles K, Schleicher A, Palomero-Gallagher N, Amunts K. 2002. Quantitative analysis of cyto- and receptor architecture of the human brain. In: Mazziotta J, Toga A, editors. Brain mapping: the methods. 2nd ed. San Diego (CA): Elsevier. p. 573–602.